Separation and Purification Technology 382 (2026) 136079

Contents lists available at ScienceDirect

Separation and Purification Technology

journal homepage: www.elsevier.com/locate/seppur

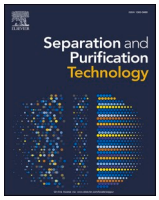

Isotherms and kinetics of CO_2 adsorption on biochar-based activated carbon for sustainable climate solutions

Selma Kuloglija [a,*], Ilias-Maximilian Kropik [a], Amal El Gohary Ahmed [a], Viktor Kalman [a], Alexander Windbacher [a], Christian Jordan [a], Aneta Konior [a], Nastaran Abbaspour [a], Noah Steinacher [a], Franz Winter [a], Daniela Tomasetig [b], Elissavet Lamprinidou [c], Michael Harasek [a]

[a] Institute of Chemical, Environmental & Bioscience Engineering E166, Technische Universität Wien, 1060 Vienna, Austria
[b] Institute of Chemical Technologies and Analytics E164, Technische Universität Wien, 1060 Vienna, Austria
[c] Department of Chemistry, Aristotle University of Thessaloniki, Thessaloniki 54635, Greece

ARTICLE INFO

Editor name: S Shouliang Yi

Keywords:
Biochar
KOH activation
Activated carbon
CO_2 capture
Isotherm modeling
Kinetic model

ABSTRACT

Increasing levels of atmospheric CO_2 are the main cause of human-induced climate change, leading to more frequent extreme weather occurrences, rising sea levels, and a decrease in biodiversity. In this light, creating effective and economical sorbents for CO_2 capture is critically important. This research involved a thorough assessment of CO_2 adsorption using KOH-activated biochars produced from pine and birch. The biomass feedstocks were carbonized at temperatures of 600 °C, 700 °C, or 800 °C and treated with KOH in a 3:1 impregnation ratio. Detailed characterization through Fourier-transform infrared spectroscopy (FTIR), N_2 physisorption (Brunauer–Emmett–Teller), Raman spectroscopy, Elemental analysis (CHNS), and scanning electron microscopy with energy-dispersive X-ray analysis (SEM-EDX) indicated that higher carbonization temperatures enhance graphitic organization, preserve a substantial number of oxygen-containing functional groups, and create primarily microporous frameworks with specific surface areas. For pine-derived activated carbon, reached a maximum of 1416 m^2/g at 800 °C, while birch-derived material achieved 1398 m^2/g at the same temperature. The equilibrium CO_2 adsorption isotherms measured at 1 bar indicated maximum capacities of 3.5 mmol/g for pine biochar and 3.2 mmol/g for birch biochar that was carbonized at 800 °C. The isotherm data is well described by the Langmuir model, implying a high affinity for CO_2 and notable monolayer capacities. Time-resolved uptake experiments demonstrate that over 90 % of the equilibrium capacity is achieved within five minutes, with characteristic half-times decreasing from approximately 1.5 min for materials carbonized at 600 °C to less than 0.8 min for those treated at 800 °C. The adsorption kinetics conform to a pseudo-first-order model, corresponding with surface-controlled physisorption behavior.

The results indicate that activating biochar via KOH at elevated temperatures produces affordable, high-surface-area biochar that can rapidly and efficiently adsorb CO_2. The differences between pine and birch, compared to the commercial coconut shell-based activated carbon, highlight the impact of precursor selection on the performance of sorbents. Collectively, these biochars have significant potential as effective, locally sourced from forestry residues, and therefore more sustainable options for carbon sequestration technologies.

1. Introduction

Climate change is becoming a global challenge, primarily due to high emissions of carbon dioxide (CO_2) in the atmosphere. This issue led the world to focus on creating effective carbon capture technologies that not only work well but are also environmentally friendly and accessible enough for everyone to use. This approach is essential for protecting our planet for future generations. The Paris Agreement reflects the international commitment to limiting global warming, aiming to restrict the increase in average temperature to no more than 1.5 °C (34.7 °F) above pre-industrial levels. Due to its considerable capacity to trap heat in the atmosphere, CO_2 accounts for approximately 79.7 % of all greenhouse

* Corresponding author.
E-mail address: selma.kuloglija@tuwien.ac.at (S. Kuloglija).

https://doi.org/10.1016/j.seppur.2025.136079
Received 29 July 2025; Received in revised form 27 October 2025; Accepted 12 November 2025
Available online 13 November 2025

gas emissions, making it particularly significant in this context [1]. Most of these emissions result from human activities, such as burning fossil fuels, clearing forests, waste incineration, and industrial operations like cement production[2,3]. In response, any meaningful mitigation strategy must focus on reducing emissions at their source and advancing technologies that can actively remove CO_2 already present in the atmosphere [4].

Despite its critical role in human socio-economic development, the utilization and dependence on fossil fuels are posing significant environmental and ecological risks, such as air pollution and degradation of the ecosystem[1]. Acknowledging these risks, the European Green Deal outlines an ambitious vision to transition the European Union into a resource-efficient and competitive economy by 2050[5]. Central to this transition are sustainable production and consumption practices, with the overarching goal of achieving climate neutrality[6,7].

Due to the exceptional textural characteristics such as extensive surface area, microporous structure, chemical stability, and effective regeneration capacity, adsorption using activated carbon (AC) has emerged as a particularly promising carbon capture method[2,3,4,8].

Biomass-derived activated carbons are increasingly recognized for their sustainability and cost-effectiveness, providing an environmentally friendly alternative to fossil-based activated carbon[1,9,10]. A significant contributor to climate change mitigation efforts is based on the facilitated utilization of waste biomass sources. Biomass such as wood, bamboo, olive pomace, banana peels, pinewood, straw, seaweed, and agricultural residues have been extensively explored as sustainable precursors for activated carbon[11,12,13,14].

Activated carbon produced from biochars derived from birch (*Betula pendula*) and pine (*Pinus sylvestris*) harvested from woodlands offers several advantages for both environmental and industrial applications. Once activated, these biochars develop a porous structure and a high surface area, allowing for adsorption of pollutants, such as dyes, heavy metals, and volatile organic compounds[15,16]. Birch and pine biochars typically have low ash content and high fixed carbon, providing the production of high-quality activated carbon with effective adsorption characteristics[17]. The improved textural and chemical properties are based on their lignocellulosic composition, which makes them particularly suited for thermal conversion and activation processes[18,19]. Additionally, utilizing locally available and renewable wood biomass supports sustainable and cost-effective production, while also promoting practices associated with the circular bioeconomy [15]. These biochars exhibit flexible surface chemistry that can be adjusted through physical/chemical activation methods to optimize performance for specific applications, such as water purification or gas adsorption [20].

Activated carbon production can be accomplished via two primary approaches: chemical and physical activation. Physical activation is a two-step sequential process, starting with the carbonization of the precursor under an inert atmosphere, followed by activation at elevated temperatures using oxidizing gases such as steam, carbon dioxide, air, or mixtures thereof [21,22,23]. Chemical activation, when compared to physical activation, presents itself to be more beneficial due to its ability to produce activated carbon with larger surface areas, enhanced pore structures, and increased carbon yields with a higher efficiency. Additionally, it operates at lower temperatures and shorter processing durations, thus offering practical advantages in terms of energy efficiency and cost-effectiveness [24,25]. The selection of activating agents significantly impacts the resulting material properties, with commonly used chemicals including potassium hydroxide (KOH)[26], phosphoric acid (H_3PO_4)[27], zinc chloride ($ZnCl_2$)[28] or sodium hydroxide (NaOH)[29], followed by carbonization.

Potassium hydroxide (KOH) activation is acknowledged for its capability of improving structural properties of biochar, specifically in terms of surface area, porosity, and CO_2 adsorption performance. During high-temperature treatment, KOH reacts with carbon matrix to produce K, K_2O, CO, and CO_2. Metallic potassium can intercalate into the carbon matrix, widening existing pores, while CO and CO_2 released during the process help create new micropores. In addition, the removal of K-containing species during the washing step leaves behind a well-developed porous structure. As a result, these combined effects explain how KOH activation tailors the pore size distribution and increases the specific surface area of the biochars. Reported specific surface areas often exceed 1500 m^2/g, and in some cases, surpass 3500 m^2/g [2,3,30,31]. Additionally, KOH activation greatly enhances carbon capture efficiency as a byproduct of its ability to facilitate the creation of micropores smaller than 0.8 nm, which demonstrate enhanced selectivity for CO_2 adsorption over other gases, such as nitrogen[12,32]. Various empirical studies have supported these findings using diverse biomass precursors. Yumak et al. showed that pine cone biochar activated with KOH had a substantial increase in specific surface area from 259.74 to 1714.5 m^2/g, resulting in a notable CO_2 adsorption capacity of 160 mg/g (3.64 mmol/g) at 25 °C [30]. Monteagudo et al. reported that activated carbon derived from rubber seed shells achieved a surface area of 1129.68 m^2/g and a maximum CO_2 adsorption capacity of 43.509 $cm^3\ g^{-1}$ at 25 °C and 1.25 bar [3]. Another study by Deng et al. using pine sawdust revealed that increasing the activation temperature from 700 °C to 900 °C significantly increased surface areas from 1728.66 to 2330.89 m^2/g, with the sample activated at 700 °C demonstrating the highest CO_2 capture capacity of 4.21 mmol/g at 298 K and 1 bar, alongside excellent stability across multiple adsorption-desorption cycles[31]. Additional research has explored various biomass sources and modifications in the activation process. Biomass-based carbon derived from black locust through KOH chemical activation, combined with ammonia modification, achieved an exceptionally high surface area of 2511 m^2/g, a large micropore volume of 1.16 $cm^3\ g^{-1}$, and substantial nitrogen content of 7.21 wt%, resulting in significant CO_2 uptakes of 7.19 mmol/g and 5.05 mmol/g at 0 °C and 25 °C, respectively [33]. Activated carbons derived from Jujun grass and *Camellia japonica* via hydrothermal carbonization followed by KOH activation exhibited surface areas ranging from 1050 to 3537 m^2/g, with CO_2 uptakes as high as 5.0 mmol/g at 1 bar and 25 °C, and notably reaching 21.1 mmol/g at 20 bar, making them suitable for both pre-and post-combustion CO_2 capture applications [34]. Sustainable porous carbons produced from polysaccharides (starch and cellulose) and sawdust, activated with KOH under mild conditions (with a KOH/precursor ratio of 2), also demonstrated high CO_2 uptake of 4.8 mmol/g at 25 °C, highlighting the importance of micropores smaller than 1 nm for effective CO_2 capture [35]. Furthermore, microporous carbon compartments (MCCs) developed from wheat flour by means of controlled carbonization exhibited significant CO_2 adsorption capacities when activated with KOH at 700 °C. The optimal KOH-to-carbon ratio was found to be 3, establishing the highest CO_2 adsorption capacity to be 5.70 mol/kg at 0 °C and 3.48 mol/kg at 25 °C. The study emphasized that CO_2 uptake efficiency is strongly correlated with the volume of narrow micropores (<0.8 nm), rather than overall surface area or larger pore volumes [36].

This research investigates the conversion of birch (*Betula pendula*) and pine (*Pinus sylvestris*), both sourced from woodlands, into biochar through the process of pyrolysis. The biochar acquired from this biomass undergoes chemical activation with potassium hydroxide (KOH). A variety of operating temperatures and impregnation ratios are investigated to enhance the production of effective activated carbon with a high BET surface area. The qualitative classification of the derived activated carbon is assessed through scanning electron microscopy (SEM), Brunauer-Emmett-Teller (BET) surface area analysis, and Fourier-transform infrared spectrometry (FTIR). In addition, this study systematically evaluated the CO_2 adsorption performance through equilibrium isotherm modeling (Langmuir) and time-resolved kinetic analysis (pseudo-first-order, pseudo-second-order, and Avrami–Erofeev models), using thermogravimetric analysis (TGA) at various CO_2 concentrations to demonstrate the promise of biomass-derived carbons for efficient and low-cost CO_2 capture.

2. Methodology

2.1. Materials

Birch (*Betula pendula*) and pine (*Pinus sylvestris*) biomass were collected from forested areas and used to produce biochar samples. The feedstock included both trunk and branch materials, which were pelletized to a uniform size of 1.5–2.5 mm prior to pyrolysis. Potassium hydroxide (KOH), sourced from Sigma-Aldrich, was employed as the chemical activating agent for biochar functionalization. Carbon dioxide (CO_2) used in the activation process was supplied by Messer Austria, with a certified high purity of 99.999 %. Nitrogen gas (N_2) was also provided by Messer Austria and of equivalent purity, and utilized during the carbonization process to convert biochar into activated carbon.

2.2. Pyrolysis process

The pyrolysis was conducted in a Nabertherm muffle furnace equipped with a chimney to facilitate a controlled removal of gaseous pyrolysis products. The furnace was preheated to 700 °C, and stable operating conditions were ensured. In this study, porcelain crucibles with lids were used since a dedicated pyrolyzer was not available. A 20 g wood pellet sample was placed into the crucible and inserted into the furnace for 10 min. Maintaining this short residence time was essential to (i) minimize oxygen intrusion, (ii) prevent partial combustion of the biomass, and (iii) preserve the resulting biochar. TGA results Supplementary Results (S1) demonstrate that a sufficient degree of pyrolysis was reached. Following the pyrolysis, in order to facilitate cooling under ambient conditions, the crucible was positioned on a heat-resistant ceramic plate for 5 min, and to prevent moisture uptake and allow it to reach room temperature, the sample was then placed in a desiccator with a drying agent for 1.5 h. Comparable short-duration pyrolysis procedures have been reported in the literature [37,38] supporting the applicability of this approach. This procedure requires that the process parameters be strictly controlled to enable accurate assessment of pyrolysis efficiency.

2.3. Chemical activation process of biochar with KOH to activated carbon

Betula pendula and *Pinus sylvestris* biochars were subjected to chemical activation using potassium hydroxide (KOH), where both materials underwent an identical preparation procedure. Primarily, the raw samples were washed with distilled water and subsequently dried to remove potential impurities. After drying, the samples were stored in a desiccator for approximately two hours before activation.

For the activation process, KOH was dissolved in distilled water to prepare solutions with impregnation ratios of 1:1, 2:1, and 3:1 (KOH: biochar, by weight). Three grams of raw biochar were added to each solution, and the mixtures were stirred continuously for 24 h to ensure thorough impregnation. The samples were filtered and dried until a constant weight was achieved. The dried impregnated biochar was placed in a quartz glass container, which was subsequently positioned inside a stainless-steel reactor, as illustrated in Fig. 1. Calcination was carried out at three different temperatures—600 °C, 700 °C, and 800 °C—for one hour, with a heating rate of 10 °C/min under a constant nitrogen flow of 200 mL/min. After cooling to room temperature, the resulting activated carbon materials were washed with 1 M hydrochloric acid (HCl). This was followed by repeated continuous rinsing with deionized water until the wash water reached a pH of approximately 7. This process was performed to remove any residual KOH and ash. Finally, all samples were dried in an oven at 105 °C for 12 h to ensure complete removal of residual moisture.

2.4. Characterization of raw biochar and activated carbon

2.4.1. CHNS elemental analysis

The elemental composition of the raw biochars, activated samples, and the commercial cylindrical activated carbon reference was determined using a Vario Macro analyzer (Elementar Analysensysteme GmbH, Germany). Each sample was analyzed using approximately 20 mg of material for the analysis. The instrument was calibrated using sulfanilamide as the daily reference standard to ensure measurement accuracy.

2.4.2. Brunauer-emmett-teller (BET) analysis

The raw biochars and activated carbon samples were degassed at a pressure of less than 10 Pa and 300 °C for 4 h, using Microtrac's BELPREP II with a rotary vane pump. Subsequently, the surface and pore characteristics of the materials were determined through N_2 adsorption measurement at 77 K utilizing the BELSORP MAX X gas adsorption device. Measurements were taken across a relative pressure range of 10–2–0.99 P/P0 to obtain adsorption and desorption isotherms. This data was used to calculate the Brunauer-Emmet-Teller (BET) surface area as well as pore volume and pore size within Microtrac's BELMASTER software. The BET surface area was determined by applying the Rouquerol criterium to the individual type I isotherms of the samples and using all points that qualified in the measured P/P_0 range. Pore size distributions were calculated by applying BELMASTER's NLDFT (nonlinear density functional theory) model for slit pores in carbon materials on the sample's isotherm. Ridge regression (also known as Tikhonov regularization) was used to obtain the final pore size distributions.

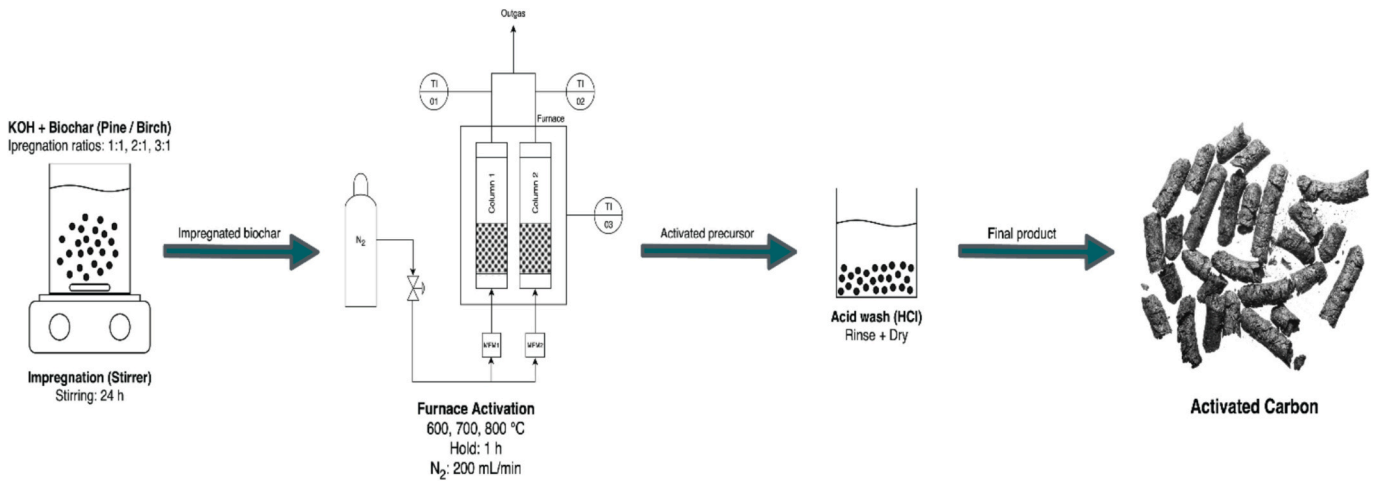

Fig. 1. Schematic of biochar activation via KOH.

2.4.3. Scanning Electron microscope (SEM)

The surface morphology of the adsorbent samples was examined using a FEI Quanta FEG 250 model Scanning Electron Microscope (SEM). Initially, the samples were mounted on aluminum stubs with carbon tape and coated with gold to affix the sample and enhance surface conductivity and electron reflection, and were treated under vacuum in the Q150T S sputter coater for around 10 min at a current intensity of 30 mA. Furthermore, energy-dispersive X-ray spectroscopy (EDX) was performed using the TEAM program for comprehensive elemental analysis.

2.4.4. Raman analysis

Raman spectra were obtained using a laser with a wavelength of 532 nm with a Witec Alpha 300RSA device. Each spectrum was integrated for 5 s, and a total of 60 spectra were accumulated per measurement. The laser power used was 10 mW, with a 10× objective.

2.4.5. Fourier-transform infrared spectroscopy (FTIR) analysis

FT-IR spectroscopy was employed to characterize the surface functional groups, such as aldehydes, carbonyls, and hydroxyls, present on both biochar and activated carbon. Spectral data were obtained in the range of 4000 to 400 cm^{-1} using a VERTEX 70 spectrometer. Each sample was scanned sixty-four times at a spectral resolution of 2 cm^{-1} to ensure high resolution and reproducibility.

2.5. CO_2 adsorption isotherms via TGA

The adsorption performance of activated biochar was systematically investigated using simultaneous thermal analysis (STA), which integrates thermogravimetric analysis (TGA) with differential scanning calorimetry (DSC). The experiments were conducted using a NETZSCH STA 449c TGA/DSC analyzer (NETZSCH-Gerätebau GmbH, Selb, Germany), with data acquisition and processing performed via the NETZSCH Proteus software (Version 8.0.2). The primary objective of this analysis was to evaluate the CO_2 adsorption capacity of activated biochar under controlled conditions, simulating dilute gas environments relevant to post-combustion carbon capture.

Adsorption experiments were performed in an inert helium (He) gas stream, serving as the carrier and protective gas, with a total gas flow rate maintained at 100 NmL/min. Carbon dioxide (CO_2) was introduced into the gas stream at varying volumetric concentrations, specifically ranging from 30 % to 75 %, to assess the effect of CO_2 partial pressure on the adsorption behavior. The biochar samples (~30 mg) were placed in 6.8 mm alumina (Al_2O_3) crucibles to ensure thermal stability and minimal interaction with the sample. All adsorption measurements were carried out isothermally at a baseline temperature of 30 °C, with additional investigations performed at elevated temperatures of 45 °C, 60 °C, and 75 °C to evaluate the temperature dependency of the CO_2 uptake and its implications for adsorption thermodynamics. At each concentration and temperature condition, a 10-min equilibration period was implemented to ensure that the system reached adsorption equilibrium before data acquisition.

This experimental design enabled a detailed examination of the influence of both CO_2 concentration and temperature on the adsorption efficiency of activated biochar. The resulting data are intended to contribute to the development of adsorption isotherm models and to provide foundational insights into the applicability of activated biochar as a low-cost, thermally stable adsorbent for carbon capture technologies.

3. Results and discussion

3.1. Characterization of biochar and activated carbon

3.1.1. Textural and morphological features (BET and SEM)

The textural properties of the raw and chemically activated biochars, along with those of a commercial activated carbon (CAC), are summarized in Table 1. These include the Brunauer–Emmett–Teller (BET) specific surface area (S_{BET}), total pore volume (V_{tot}), and average pore diameter (D_{dp}).

The raw biochars derived from pine and birch present relatively low surface areas of 313 m^2/g and 351 m^2/g, respectively. Chemical activation with KOH at an impregnation ratio of 3:1 (wt/wt) led to significant enhancements in both surface area and porosity, particularly at activation temperatures of 700 °C and 800 °C (full data for all tested KOH:biochar ratios are provided in Supplementary Material (ST1). Based on preliminary investigations, the 3:1 ratio yielded the highest BET surface area among the tested ratios for both pine and birch biochars, and also exceeded the surface area of the commercial activated carbon, justifying its selection for detailed study in the main manuscript. For example, pine-derived activated carbon reached a maximum surface area of 1416 m^2/g at 800 °C, while birch-derived material achieved 1398 m^2/g at the same temperature—both surpassing the surface area of the commercial activated carbon (1023 m^2/g). These increases were accompanied by higher total pore volumes (up to 0.59 $cm^3\ g^{-1}$ for pine and 0.58 $cm^3\ g^{-1}$ for birch) and slightly reduced average pore diameters, suggesting the development of a predominantly microporous structure. Although the average pore diameter remained similar across samples (~0.83 nm), the substantial rise in surface area indicates a greater concentration of micropores in the lab-prepared biochars.

Notably, activation of birch biochar at 600 °C resulted in a surface area (263 m^2/g) lower than that of its raw biochar (351 m^2/g). The SEM image (Fig. 3-g) clearly shows significantly reduced porosity and evidence of incomplete activation. This indicates that the lower surface area is primarily due to insufficient development of the carbon structure. While pore blockage or minor structural collapse during activation cannot be fully ruled out, incomplete activation appears to be the main factor limiting pore formation at this temperature.

The N_2 adsorption–desorption isotherms for the pine-derived activated carbon (Fig. 2-a) exhibit a Type I behavior, suggesting that pore filling within predominantly microporous structures regulates the uptake process. The untreated pine biochar demonstrates a limited uptake, suggesting its porosity is poorly developed. Activation at 600 °C nearly doubles the available pore volume, while activation at 700 °C further enhances it to approximately 270 $cm^3\ g^{-1}$. The sample treated at 800 °C achieves the highest overall uptake, reaching around 380 $cm^3\ g^{-1}$, thereby exceeding even the commercial activated carbon reference, which is about 280 $cm^3\ g^{-1}$. In all activated pine samples, the sharp increase in uptake at very low relative pressures ($p/p_o < 0.1$) confirms the formation of numerous narrow micropores. At the same time, the nearly horizontal plateau beyond $p/p_o \approx 0.3$ indicates that minimal additional mesoporosity is developed.

Overall, these results demonstrate that consistently increasing the activation temperature modifies the pore structure and significantly improves the specific pore volume of pine biochar, with treatment at 800 °C yielding a micropore-rich material that outperforms the

Table 1
BET surface area, total pore volume, and average pore diameter of pine- and birch-derived biochars before and after activation, compared with commercial activated carbon.

Sample	S_{BET} (m^2/g)	V_T ($cm^3\ g^{-1}$)	D_{pd} (nm)
Pine biochar	313	0.15	0.94
Birch biochar	351	0.16	0.91
Impregnation ratio 3:1 (wt/wt) activation temperature (°C)			
Pine 600 °C	496	0.23	0.94
Pine 700 °C	1093	0.46	0.84
Pine 800 °C	1416	0.59	0.84
Birch 600 °C	263	0.13	0.95
Birch 700 °C	1014	0.42	0.83
Birch 800 °C	1398	0.58	0.83
Commercial activated carbon	1023	0.44	0.85

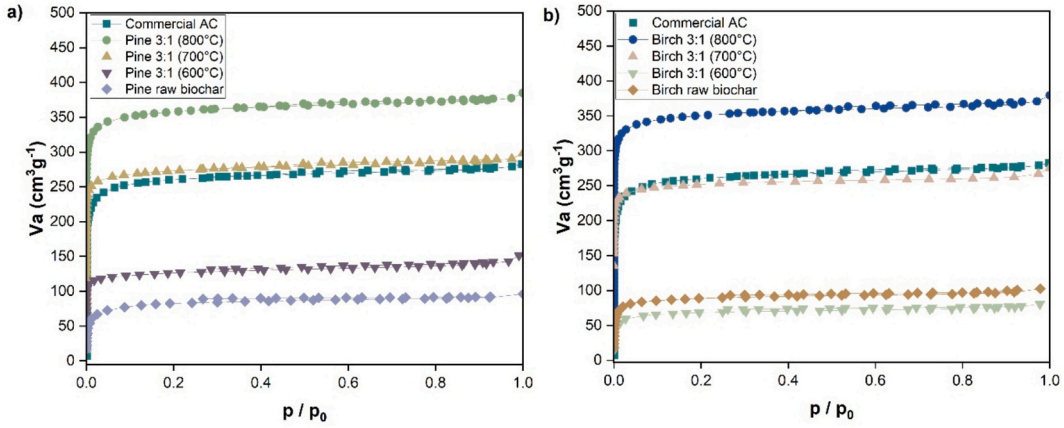

Fig. 1. Nitrogen adsorption isotherms (adsorption branch) of raw and KOH-activated biochars measured at 77 K. (a) Pine-derived samples: raw biochar (◆), 3:1 KOH:biochar activation at 600 °C (▼), 700 °C (▲) and 800 °C (●), alongside a commercial activated carbon reference (■). (b) Birch-derived samples: raw biochar (◆), 3:1 KOH:biochar activation at 600 °C (▼), 700 °C (▲), and 800 °C (●), alongside the same commercial activated carbon reference (■). Adsorbed volume, Va ($cm^3\ g^{-1}$), is plotted against relative pressure, p/p_o.

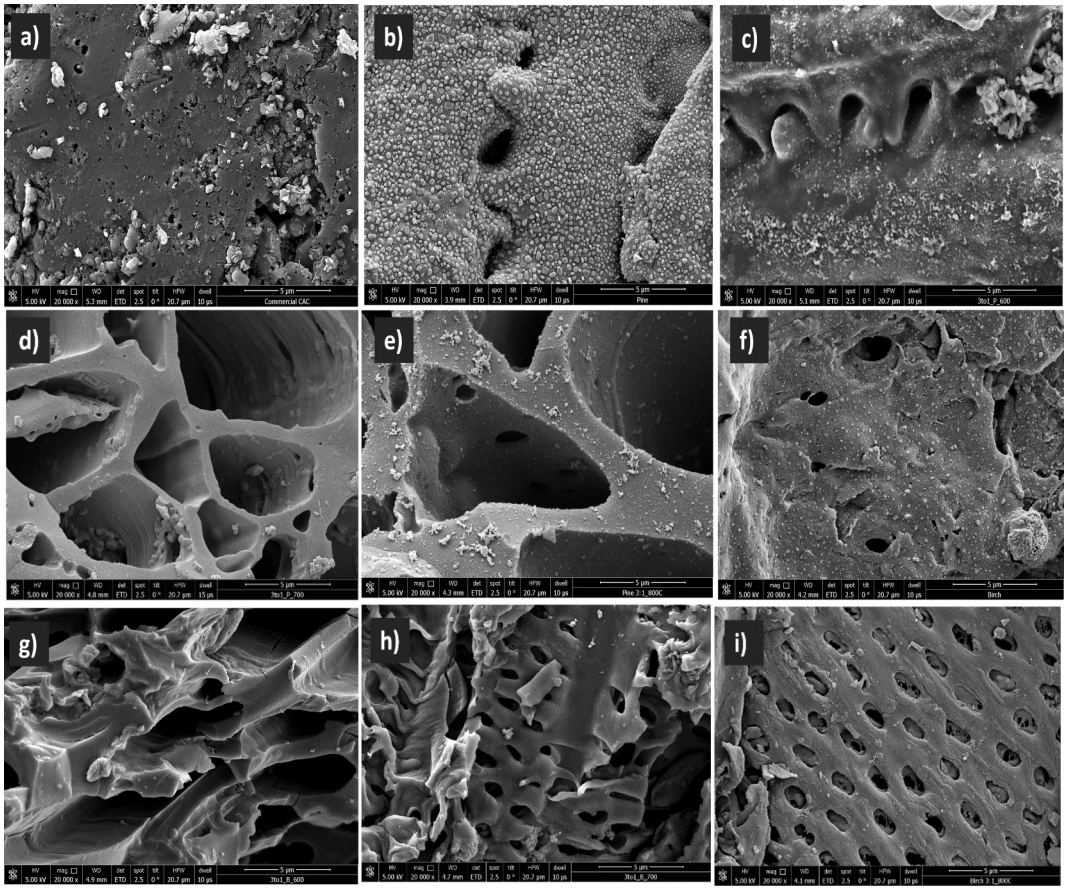

Fig. 3. Scanning-electron micrographs (SEM) of commercial activated carbon and KOH-activated biochars derived from pine and birch. A) Commercial activated carbon; b) raw pine biochar; c) pine biochar activated (3:1 KOH:biochar) at 600 °C; d) activated at 700 °C; e) activated at 800 °C; f) raw birch biochar; g) birch biochar activated (3,1 KOH:biochar) at 600 °C; h) activated at 700 °C; i) activated at 800 °C.

commercial reference. The N_2 adsorption and desorption isotherms of the activated carbon derived from birch (Fig. 2-b) represents typical Type I characteristics, indicating a predominantly microporous structure.

A notable increase in adsorption is observed at 700 °C, where it reaches approximately 250 $cm^3\ g^{-1}$, which is comparable to the commercial activated carbon (around 260 $cm^3\ g^{-1}$).

Finally, treatment at 800 °C results in the highest adsorption capacity, approximately 350 $cm^3\ g^{-1}$, substantially higher than the adsorption capacity of commercial activated carbon. In all activated birch samples, the noticeably steep increase in adsorption at very low relative pressures ($p/p_o < 0.1$) confirms the formation of a large number of narrow micropores, while the plateau observed after $p/p_o \approx 0.3$ indicates that minimal additional mesoporosity is developed. The

activation of both pine and birch at 700 °C and 800 °C leads to significant improvements due to the formation of abundant micropores.

The analysis of pore size distribution supports these findings. The ultra-micropore volume

(< 0.7 nm) was quantified, and the corresponding MP plots are provided in the Supplementary Material (S2). For the 3:1 KOH-activated pine and birch biochars, compared with the commercial activated carbon, all samples (except birch 3:1 at 600 °C) exhibit a pronounced peak at approximately 0.6 nm in the MP plot, indicating a concentration of ultra-micropores, which strongly supports their suitability for CO_2 adsorption.

To gain further insight into surface area development, the surface morphology of the samples was characterized using scanning electron microscopy (SEM). As shown in Fig. 3, all materials—including the commercial activated carbon—display heterogeneous and irregular surface textures typical of carbonaceous materials. The surface features of the KOH-activated biochars, particularly those treated at 700 °C and 800 °C, are more developed, showing a distinctly porous structure with a wide variety of pore sizes and shapes. These textural differences suggest that KOH activation significantly enhances pore development compared to both the raw biochars and the commercial reference material.

The raw pine biochar (Fig. 3b) displays a relatively impure surface, characterized by residual biomass deposits and uneven texture as confirmed by energy dispersive analysis (EDX) in paragraph 3.1.3. Following KOH activation at 600 °C (Fig. 3c), partial degradation of the carbon matrix becomes evident, leading to the formation of small surface indentations and a cleaner, more structured appearance. Increasing the activation temperature to 700 °C (Fig. 3d) leads to the formation of a network of interconnected mesopores, while activation at 800 °C (Fig. 3e) further enhances this network into a hierarchically porous structure with extensive pore development.

A comparable trend is observed in birch-derived biochars. The raw birch biochar (Fig. 3f) also shows an impure surface with only a few visible pores, indicating limited porosity and minimal structural development at this stage. Activation at 700 °C (Fig. 3h) generates a heterogeneous distribution of medium-sized pores, whereas treatment at 800 °C (Fig. 3i) results in the formation of a well-developed, uniform array of rounded pores. These morphological transformations reflect the progressive influence of KOH activation on the biochar matrix, which becomes increasingly porous with rising temperature[39]. Despite showing similar trends, both biochars and their final pore structures remain feedstock-dependent.

This behavior can be attributed to the chemical interactions between KOH and carbon at elevated temperatures. Above 600 °C, KOH begins to react with the carbon matrix according to Eqs. (1)–(5), initiating pore formation. At higher temperatures (700–800 °C), KOH melts and reacts more significantly with biochar, producing potassium-containing species such as K_2CO_3, K_2O, and metallic K[3]. These species contribute to the chemical etching and structural corrosion of the carbon surface, which promotes the development of porosity, as reflected in the increased surface area values reported in Table 1.

$$2\,KOH \leftrightarrow K_2O + H_20 \quad (1)$$

$$6KOH + 2\,C \rightarrow 2\,K + 3H_2 + 2K_2CO_3 \quad (2)$$

$$K_2CO_3 \leftrightarrow K2\,O + CO_2 \quad (3)$$

$$K_2CO_3 + 2\,C \rightarrow 2\,K + CO \quad (4)$$

$$K_2O + C \rightarrow 2\,K + CO \quad (5)$$

The resulting irregular and microporous morphology significantly enhances the material's suitability for gas-phase adsorption, particularly for CO_2 molecules. Among all tested samples, the 3:1 KOH-activated biochars treated at 800 °C—derived from both pine (Fig. 3e) and birch (Fig. 3i)—exhibited the most developed, hierarchical pore networks, showing significant improvements in textural and adsorption properties compared to the selected commercial activated carbon.

3.1.2. Characterization of surface chemistry and functional groups (FTIR and Raman)

The spectral analysis of both pine- and birch-derived raw and activated biochars, as well as commercial activated carbons in Fig. 4-a, provides insight into the evolution of surface functional groups as a function of activation temperature. In the presented spectra, the vertical axis represents the transmittance of surface bonds, while the horizontal axis corresponds to the wavenumber (cm^{-1}).

In both series (a and b), a broad absorption band centered around 3700 cm^{-1} is observed, attributed to O—H stretching vibrations of hydroxyl groups. This feature is more pronounced in commercial activated carbon and in samples of birch and pine activated at 700 °C and 800 °C, compared to raw biochar and samples activated at 600 °C. This enhancement is likely due to the activation process, which increases the surface area and introduces a greater quantity of oxygen-containing functional groups, particularly hydroxyl groups. The band observed near 2347 cm^{-1}, associated with C≡C stretching vibrations of alkynes, is faint or absent in the raw materials but becomes more distinct in samples activated at 700 °C and 800 °C [40]. This suggests the formation of more ordered carbon structures at elevated temperatures, especially notable in the pine samples, where the sharper band indicates a higher degree of graphitization. This observation aligns with Raman spectroscopy data in Fig. 4-b, in which the intensity ratio of the D and G bands (I_D/I_G) is 0.96996, confirming a greater proportion of ordered carbon structures.

Additionally, bands in the 1700–1600 cm^{-1} region, corresponding to C═O stretching vibrations of carbonyl groups common in activated carbons post-modification or oxidation, are more intense in commercial activated carbon and in birch and pine activated at 700 °C and 800 °C [11,39]. In contrast, these bands are weaker in raw biochar and in samples activated at 600 °C. The presence of these carbonyl functionalities plays a critical role in determining the adsorption and catalytic behavior of the material. The peak around 1570 cm^{-1}, associated with C═C stretching in aromatic systems, is also more intense in commercial activated carbon and in treated pine and birch samples at 700 °C and 800 °C. This increase suggests a higher degree of aromatic character and ordering of carbon atoms. C—O stretching vibrations, typically observed near 1100 cm^{-1} and associated with alcohol, ether, or ester functionalities, exhibit a reduction in intensity with increasing activation temperature. This trend further supports the notion of progressive removal of surface oxygen-containing groups. In the fingerprint region (750–600 cm^{-1}), bands related to C—H bending vibrations are also observed [3,40].

Overall, both pine and birch samples exhibit similar qualitative trends in the evolution of surface functional groups with increasing activation temperature. Notably, samples activated at 700 °C and 800 °C demonstrate significant transformations that closely resemble the characteristics of commercial activated carbon. The observed decline in O—H, C═O, and C—O bands, coupled with the emergence of more prominent C≡C and aromatic C—H bands, indicates more efficient carbonization and graphitization processes at higher activation temperatures.

Thus, activated pine and birch samples at 800 °C appear particularly well-suited for the production of high-performance activated carbon materials. These materials exhibit higher aromaticity, reduced surface oxygen content, and potentially improved thermal and chemical stability—traits that are advantageous for applications such as adsorption, catalysis, and energy storage. Active surface groups can be qualitatively analyzed with various methods such as Boehm titration, Raman spectroscopy or FTIR. In this work, FTIR and Raman were selected for the first preliminary investigation, as the Boehm titration does not give significantly improved results [41], while the effort is much higher.

Fig. 5 illustrates the Raman spectra of two raw biochars, their

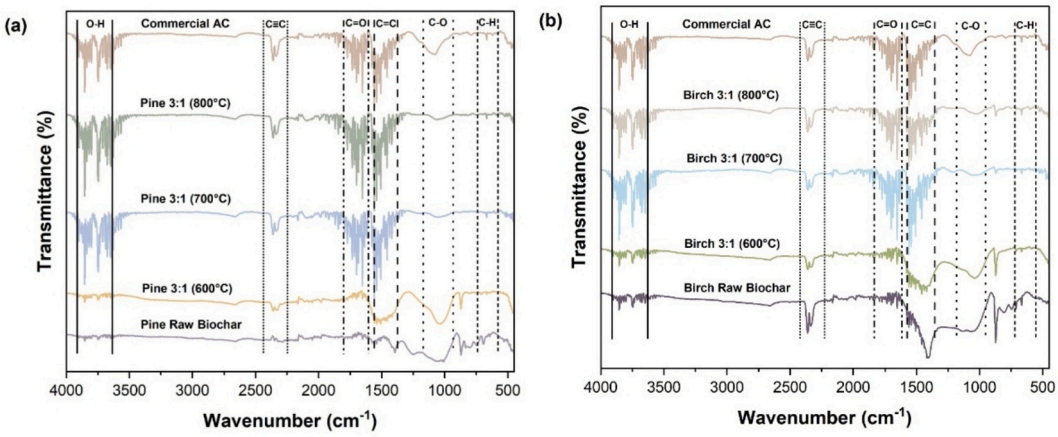

Fig. 4. (a) FTIR spectra of commercial activated carbon, raw pine biochar, and KOH-activated pine biochar at an impregnation ratio of 3:1 and temperatures of 600 °C, 700 °C, and 800 °C; (b) FTIR spectra of commercial activated carbon, raw birch biochar, and KOH-activated birch biochar at an impregnation ratio of 3:1 and temperatures of 600 °C, 700 °C, and 800 °C.

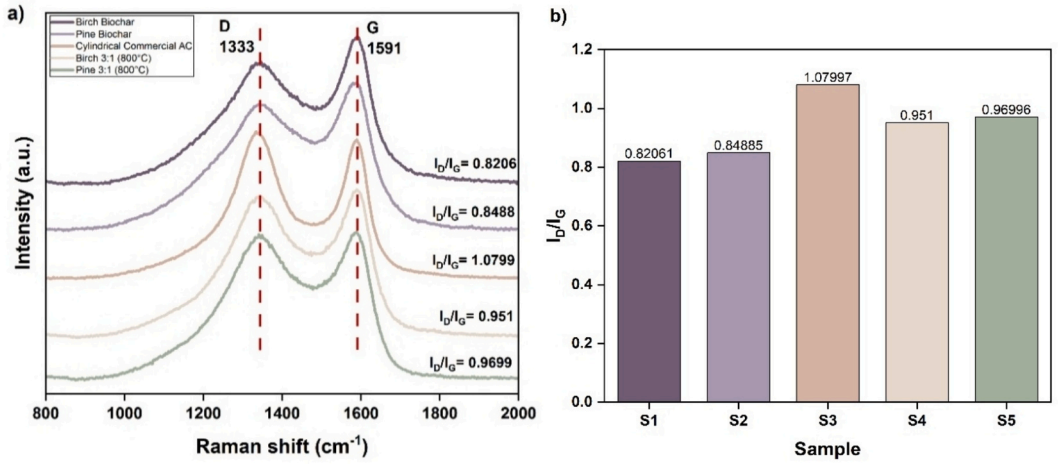

Fig. 5. (a) Raman spectra of selected samples; (b) D/G peak area ratio of different samples: S1 – Birch biochar (raw); S2 – Pine biochar (raw); S3 – Commercial activated carbon; S4 – Birch 3:1 (800 °C); S5 – Pine 3:1 (800 °C).

activated forms obtained at 800 °C with an impregnation ratio of 3:1, and a commercial cylindrical activated carbon, in the spectral range of 800–2000 cm^{-1}. Raman spectroscopy is used to analyze the structural characteristics and degree of disorder in carbon materials.

In this analysis, the characteristic peak at 1333 cm^{-1}, known as the D peak, represents the disordered structure of carbon, indicating the degree of structural defects and the presence of impurities. In contrast, the peak at 1591 cm^{-1}, referred to as the G peak, corresponds to the graphitized structure of carbon, reflecting a more ordered, symmetrical, and crystalline arrangement, which is essential for high-quality carbon materials [42,43]. As shown in Fig. 5-b, the intensity ratio of the D band to the G band (I_D/I_G) was calculated to assess the degree of structural order in the carbon materials. For the raw biochar samples, the birch biochar (S1) exhibits an intensity ratio of 0.8206, while the pine biochar (S2) shows a ratio of 0.8488, both indicating a high degree of graphitization and relatively low disorder.

After activation at 800 °C with an impregnation ratio of 3:1, the intensity ratios increased. The activated birch biochar (S4) shows an intensity ratio of 0.951, and the activated pine biochar (S5) also displays an increase, indicating that activation at higher temperatures introduces more structural defects.

In comparison, the commercial cylindrical activated carbon (S3) exhibits the highest intensity ratio of 1.0799, suggesting a higher degree of disorder and a greater presence of defective carbon structures. Both activated biochars (S4 and S5) maintain I_D/I_G ratios below 1, indicating a higher proportion of ordered carbon structures compared to the commercial activated carbon [43,44]. This is consistent with the observations in Section 3.1.1, where SEM images revealed a more regular morphology and a continuously oriented porous structure in the activated biochars.

3.1.3. Elemental and chemical composition(CHNS and EDX)

Table 2 presents the elemental surface composition, highlighting a higher graphitic purity of KOH-activated biochars in comparison to commercial activated carbon. Birch biochar activated at 800 °C with a 3:1 KOH:biochar ratio shows an increase in carbon content from 80.5 wt

Table 2
Elemental Composition of Biochars Derived from Birch and Pine, and a Commercial Activated Carbon.

Sample	N	C	H	S	O/C	H/C
Birch raw	1.76	80.54	1.81	0.15	0.15	0.27
Birch 3:1 (800 °C)	0.89	90.22	0.44	0.12	0.07	0.06
Pine raw	0.67	67.34	1.41	0.83	0.34	0.25
Pine 3:1 (800 °C)	1.04	89.59	0.47	0.22	0.07	0.06
Commercial AC	0.36	87.69	0.09	0.49	0.09	0.01

% to 90.2 wt%, exceeding that of the commercial activated carbon (87.7 wt%). Similarly, pine biochar increases its carbon content from 67.3 wt % to 89.6 wt%. Both activated biochars demonstrate substantial reductions in hydrogen content (from approximately 1.8 wt% to 0.4 wt% for birch, and from 1.4 wt% to 0.5 wt% for pine), as well as notable decreases in nitrogen and sulfur impurities, indicating the thermal volatilization of heteroatom-containing functional groups [42]. Overall, the activated biochars—particularly those derived from birch—achieve carbon purities and residual ash levels comparable to or surpassing those of the commercial reference material, underscoring their strong potential as highly conductive and efficient adsorbents.

The Van Krevelen diagram is employed to illustrate the reduction and transformation of carbon, oxygen, and hydrogen contents during the carbonization process of biochars (Fig. 6). The degree of carbonization is represented by the relative position of data points on the diagram, with greater distances indicating more intense carbonization. Activated biochars derived from birch and pine are located in the lower left region of the diagram, indicating a high degree of carbonization, elevated aromaticity, and enhanced thermal stability. Notably, carbon content is a crucial parameter for evaluating the degree of carbonization and the formation of aromatic structures. As shown in Table 2, elemental analysis of biochars produced from pine and birch at 800 °C reveals significantly increased carbon contents, 89.6 % for pine and 90.2 % for birch, which corresponds with decreased H/C and O/C molar ratios, confirming enhanced aromaticity and thermal resistance.

Initially, birch exhibits a higher carbon content and a lower O/C ratio compared to pine; however, after activation, both biochars converge toward the graphitic region of the diagram, indicating successful transformation into high-purity activated carbons, comparable to commercial-grade materials. Conversely, raw biomass-derived biochars display higher H/C and O/C ratios along with lower carbon contents—80.5 % for birch and 67.3 % for pine—indicative of limited carbonization and a predominance of aliphatic and oxygenated functional groups. These chemical characteristics contribute to increased hydrophilicity and polar surface interactions but compromise structural integrity and specific surface area [45,46].

To identify the elemental composition of the materials, the energy dispersive X-ray (EDX) analysis was conducted. This remarkable demineralization and deoxygenation result in a highly graphitic, defect-rich framework with clear pore channels, which, combined with its hierarchically organized porosity, provides expected electrical conductivity, chemical durability, and adsorption efficacy within the series. Detailed elemental compositions for all samples, including commercial activated carbon, are provided in the Supplementary Material (S3).

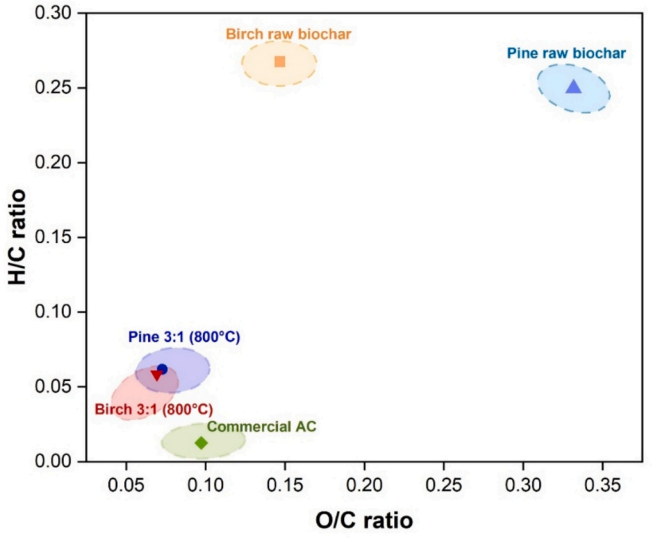

Fig. 6. Van Krevelen Diagram for Birch and Pine biochars (Raw & Activated).

3.2. CO_2 adsorption performance of activated carbon

3.2.1. CO_2 adsorption isotherms of pine-, birch-derived, and commercial activated carbons at 30 °C

CO_2 adsorption isotherms for both pine- and birch-derived activated carbons—chemically activated with KOH at a 3:1 impregnation ratio, carbonized at 600 °C, 700 °C, and 800 °C—were systematically investigated and compared against a commercial activated carbon (AC).

The adsorption isotherms for pine-800 and birch-800 displayed steep initial slopes indicative of high CO_2 affinity. To describe this behavior quantitatively, the Langmuir model was applied:

$$q_i = q_{max}\frac{bp_i}{1+bp_i} \tag{6}$$

where:

- q_i = the absolute amount adsorbed (mmol/g)
- q_{max} = maximum monolayer adsorption capacity based on the Langmuir model (mmol/g)
- b = affinity constant (bar^{-1})
- p_i = equilibrium CO_2 pressure (bar)

The Langmuir model is frequently used for microporous carbon systems because it assumes a homogeneous surface with monolayer physical adsorption—an assumption validated by the high R^2 values ($\geq$0.99) obtained for all samples.

As shown in Fig. 7, the adsorption capacity of all biomass-derived samples increased significantly with activation temperature, indicating that thermal treatment and chemical activation are crucial for developing effective porous networks. At 800 °C, pine-800 demonstrated the highest CO_2 uptake (~3.50 mmol/g at 0.9 bar), closely followed by birch-800 (~3.10 mmol/g). Pine-700 and birch-700 registered moderate uptakes (~2.2–2.4 mmol/g), while pine-600 and birch-600 remained below 1.5 mmol/g. The commercial AC, by comparison, showed a markedly lower capacity of ~1.52 mmol/g under identical conditions. These results align with previous findings that KOH activation at higher temperatures is highly effective in generating ultramicropores, which greatly enhance CO_2 adsorption.

Pine-800, with the most abundant and strongest adsorption sites, exhibited the highest q_{max} and affinity constant, outperforming Birch-800, which was slightly less effective, and commercial AC, which showed roughly half the q_{max} and a lower b (Table 3), underscoring the

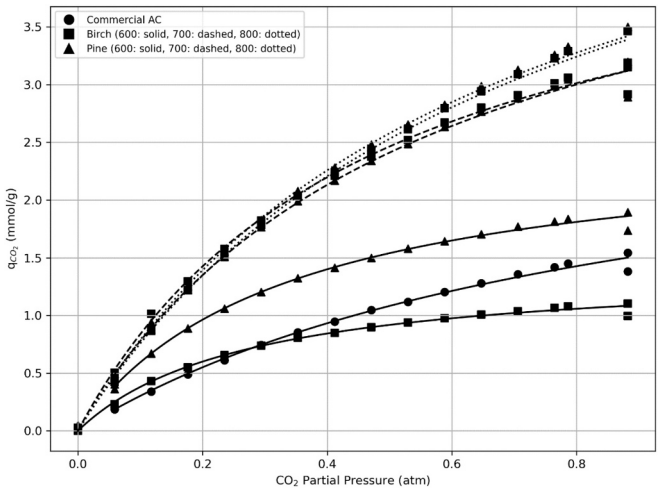

Fig. 7. Experimental and Langmuir-Fitted CO_2 Adsorption Isotherms of Pine-, Birch-Derived, and Commercial Activated Carbons at 30 °C.

Table 3
Fitted Langmuir model parameters for CO_2 adsorption at 30 °C on commercial activated carbon and biochars derived from birch and pine at 600, 700, and 800 °C.

Sample	q_{max} (mmol/g)	b (bar $^{-1}$)	R^2
Birch 3:1 (600 °C)	1.46627	3.30451	0.99928
Birch 3:1 (700 °C)	5.02763	1.86625	0.99906
Birch 3:1 (800 °C)	6.51888	1.26018	0.99979
Pine 3:1 (600 °C)	2.64233	2.95099	0.99961
Pine 3:1 (700 °C)	5.25352	1.79214	0.99969
Pine 3:1 (800 °C)	6.44587	1.27634	0.99979
Commercial AC	3.26874	1.00696	0.99962

value of KOH activation and high-temperature treatment for producing high-performance CO_2 adsorbents.

Textural characterization by N_2 adsorption–desorption (BET) isotherms reveals that Pine-800 exhibits the largest surface area (1416 m^2/g) and micropore volume (0.591 $cm^3\ g^{-1}$), with a pore structure rich in ultra-micropores that closely matches the 0.33 nm diameter of CO_2 molecules. Birch-800 follows closely, exhibiting a BET surface area of 1398 m^2/g and a micropore volume of 0.582 $cm^3\ g^{-1}$, whereas the commercial activated carbon shows markedly lower values (1023 m^2/g and 0.436 $cm^3\ g^{-1}$, respectively). These findings corroborate the well-established conclusion that high ultra-microporosity rather than total surface area alone is the primary factor driving enhanced CO_2 uptake at low pressures.

The isosteric heat of adsorption (ΔH) obtained from the Clausius–Clapeyron relation provides an indirect thermodynamic estimation of the interaction strength between CO_2 molecules and the adsorbent surface, reflecting equilibrium adsorption energetics rather than the actual energy required for thermal regeneration. In this study, ΔH was evaluated using the Clausius–Clapeyron approach applied to Langmuir fits obtained at 30, 45, 60, and 75 °C (303–348 K).

To ensure consistent comparison and to avoid artifacts near saturation, the loading was fixed at 60 % of the lowest *q_max* among the four temperatures for each sample. The corresponding equilibrium pressures were calculated from the inverted Langmuir equation, and ln*p* was plotted against $1/T$. Linear regression provided the slope, from which ΔH was determined as $-R\cdot\{slope\}$. Across the eleven investigated carbons, the heat of adsorption ranged from 16.6 to 29.4 kJ mol^{-1}, with a median of 26.5 kJ mol^{-1} as presented in Table 4. These values fall within the range expected for physisorption of CO_2 on activated carbons and highlight the consistent adsorption energetics across the biomass-derived samples.

3.2.2. CO_2 adsorption isotherms of a KOH-activated pine biochar, impregnated at a 3:1 KOH-to-carbon ratio and activated at 800 °C

Pine-derived activated carbon, prepared at a mass impregnation ratio of 3:1 and activated at 800 °C, was tested for CO_2 adsorption at 30 °C, 45 °C, 60 °C, and 75 °C over a partial pressure range up to approximately 0.9 bar. All isotherms in Fig. 8 show a steep initial rise at

Table 4
Isosteric heat of CO_2 adsorption (ΔH) of pine- and birch-derived biochars and commercial activated carbon, calculated using the Clausius–Clapeyron method.

Sample	$\Delta H\ (J/mol)$	R^2
Birch	27,498	0.976
Birch-600-1to1	22,249	0.984
Birch-600-3to1	16,560	0.895
Birch-700-3to1	29,441	0.999
Birch-800-3to1	29,448	0.997
Pine	26,322	0.975
Pine-600-1to1	20,020	0.962
Pine-600-3to1	26,029	0.996
Pine-700-3to1	29,227	0.999
Pine-800-3to1	28,840	0.997
Commercial activated carbon	26,510	0.988

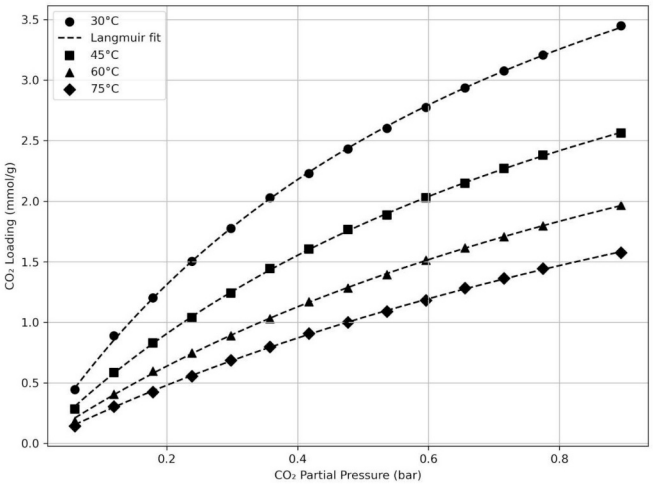

Fig. 8. CO_2 adsorption isotherms of a KOH-activated pine biochar, impregnated at a 3:1 KOH-to-carbon ratio and activated at 800 °C.

low pressure, typical of Type I behavior. The isotherm shape indicates micropore filling and physisorption typical of high-temperature KOH activation. The decrease in adsorption capacity with increasing temperature further corroborates the exothermic nature of CO_2 physisorption, wherein high thermal energy disrupts adsorbate-adsorbent interactions and reduces CO_2 uptake efficiency.

As the temperature for adsorption increases from 30 °C to 75 °C, the CO_2 uptake by pine-derived activated carbon (pine-800) declines markedly from approximately 3.54 mmol/g at 30 °C to 1.60 mmol/g at 75 °C highlighting the exothermic nature of physisorption: elevated temperatures boost the kinetic energy of CO_2 molecules, weakening their interactions with microporous surfaces [47].

The data were fitted using the Langmuir model (Eq. 6). Across all measured temperatures, the model achieved excellent fits ($R^2 > 0.995$), confirming that CO_2 adsorption occurs predominantly through monolayer coverage on a homogeneous distribution of micropores.

As the temperature increased, both the Langmuir monolayer capacity (q_m) and the affinity constant (b) decreased, indicating fewer available adsorption sites and weaker CO_2 adsorbent interactions [42].

Similarly prepared pine-800 carbons (activated at 800 °C with KOH) exhibit BET surface areas of roughly 1200 m^2/g and micropore volumes of 0.48–0.55 $cm^3\ g^{-1}$ [48]. Their ultra-micropores (< 0.7 nm) generate overlapping adsorption potential fields that significantly enhance CO_2 uptake at low partial pressure [49].

Beyond its well-developed microporous structure, residual surface functional groups—particularly hydroxyl (–OH) and carbonyl (C=O) moieties—introduced or retained during KOH activation contribute to increased surface polarity.

Pine-800 exhibits robust and thermally stable CO_2 adsorption behavior that closely conforms to Langmuir monolayer adsorption mechanisms. Its high monolayer capacity ($q_{max} \approx 6.45$ mmol/g) and strong adsorption affinity (b ≈ 1.3 bar) at 30 °C, as shown in Table 5, underscore its effectiveness for post-combustion CO_2 capture, where low-pressure, ambient-temperature operation is typical. It was noticed that the material maintains appreciable adsorption capacity even at

Table 5
Langmuir parameters for CO_2 adsorption on the pine-800 °C (3:1; KOH:biochar) sample at varying temperatures.

Temperature (°C)	q_{max} (mmol/g)	b (bar $^{-1}$)	R^2
30	6.44587	1.27634	0.99979
45	5.4526	0.99549	0.99982
60	4.9153	0.74404	0.99965
75	4.7088	0.5662	0.99972

elevated temperatures, retaining approximately 1.6 mmol/g at 75 °C—highlighting its practical resilience and potential for deployment in industrial carbon capture scenarios subject to thermal fluctuations.

3.2.3. CO_2 adsorption isotherms of a KOH-activated birch biochar, impregnated at a 3:1 KOH-to-carbon ratio and activated at 800 °C

Fig. 9 shows the CO_2 adsorption isotherms of birch-derived activated carbon (KOH-activated at a 3:1 ratio and carbonized at 800 °C), measured at 30, 45, 60, and 75 °C over CO_2 partial pressures up to ~0.9 bar. A Type I isotherm was observed, indicating microporous CO_2 adsorption. As the temperature increased, CO_2 uptake decreased systematically, from a maximum of approximately 3.5 mmol/g at 30 °C to around 1.5 mmol/g at 75 °C. This inverse relationship matches the expectation of thermodynamics of exothermic physisorption, wherein higher thermal energy reduces the interaction strength between CO_2 molecules and the adsorbent surface, thereby shifting the adsorption equilibrium unfavourably.

The Langmuir equation, as previously defined, was fitted to the experimental CO_2 isotherms obtained at all four temperatures. The resulting dashed curves in Fig. 9 exhibit strong agreement with the experimental data across the entire pressure range, confirming that monolayer adsorption is the dominant mechanism under the studied conditions. The model's high correlation coefficients ($R^2 > 0.99$) support the appropriateness of this approach. The corresponding Langmuir parameters are presented in Table 6.

Both the (q_{max}) and the (b) exhibited a systematic decline with increasing temperature, highlighting the thermodynamic weakening of CO_2 adsorption interactions at elevated thermal conditions. This behavior is characteristic of physisorption, wherein increased molecular kinetic energy at higher temperatures reduces the residence time of CO_2 on adsorption sites, shifting the equilibrium toward desorption.

This behavior is consistent with previous research demonstrating that KOH activation markedly enhances microporosity, which in turn improves CO_2 adsorption performance. Specifically, activation at high temperatures such as 800 °C has been shown to facilitate the development of a well-connected network of ultra-micropores, which are highly effective for CO_2 capture.

The pronounced steepness of the initial isotherm slopes at low CO_2 partial pressures—particularly evident at 30 °C—highlights the strong affinity of the KOH-activated birch carbon for CO_2, even under sub-atmospheric conditions. This behavior reflects the dominance of ultra-microporous adsorption, where narrow pore diameters and enhanced interaction potentials contribute to efficient capture at low concentrations.

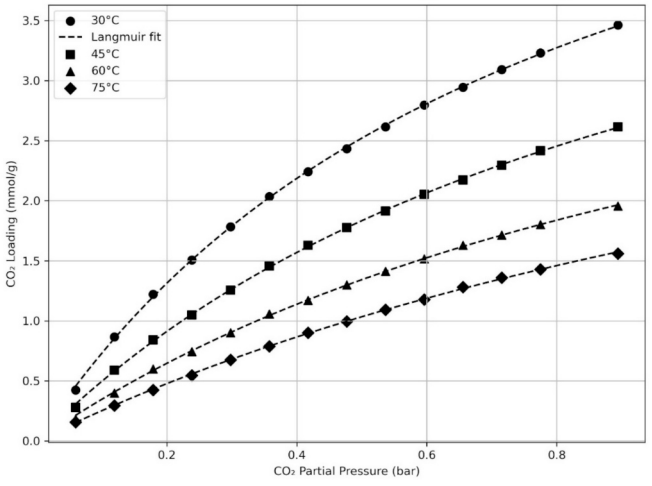

Fig. 9. CO_2 adsorption isotherms of a KOH-activated birch biochar, impregnated at a 3:1 KOH-to-carbon ratio and activated at 800 °C.

Table 6
Langmuir parameters for CO_2 adsorption on the birch-800 °C sample at varying temperatures.

Temperature (°C)	q_{max} (mmol/g)	b (bar $^{-1}$)	R^2
30	6.5188	1.26018	0.99979
45	5.63142	0.96485	0.99977
60	4.77699	0.781	0.9996
75	4.67253	0.56756	0.99971

Temperature demonstrates a role in determining the retention of adsorption capacity, as increasing the temperature can weaken physisorptive interactions. Langmuir isotherm provides a robust and reliable framework for characterizing the equilibrium adsorption behavior, capturing the temperature-dependent shifts in both adsorption capacity and affinity within this microporous system.

To provide context for the CO_2 adsorption capacity, in this study a comparative analysis was performed between the present biochars and other KOH-activated carbons reported in the literature Table 7. The pine and birch biochars in this work show CO_2 uptakes of 3.5 and 3.4 mmol/g, with specific surface areas of 1416 and 1398 m^2/g. The values mentioned are slightly lower compared to activated carbons derived from palm shells, pine cones, and rice husk, which exhibit higher CO_2 uptakes (4.4, 3.6, and 3.7 mmol/g) and larger surface area (1890, 1715, and 2695 m^2 /g).

The surface chemical composition contributes to the affinity for CO_2. The current biochars are rich in oxygen-containing groups (O—H, C═O, C—O), which enhance CO_2 interaction through dipole–quadrupole forces. In this study, the slightly lower CO_2 uptake is likely due to a smaller total pore volume and a lack of chemically active surface features.

Compared to surface area, the total pore volume (V_T) is an important factor affecting CO_2 adsorption, which represents the total internal space within the material, where gas molecules can be stored. A higher V_T means that the material contains more pores and a greater overall void volume, allowing it to accommodate more CO_2 molecules and enabling easier gas diffusion through the pore network.

The pine and birch biochars in this study have V_T values of 0.59 and 0.58 $cm^3\ g^{-1}$, which are somewhat lower than those reported for other activated carbons (0.53–1.14 $cm^3\ g^{-1}$). This indicates that although our samples possess high surface area, they contain a smaller fraction of larger micropores and mesopores that contribute to total pore volume. As a result, the overall CO_2 uptake is slightly lower, since the total available pore space for adsorption is more limited.

The developed microporous structure and high surface area indicate good potential for CO_2 capture, and further enhancement could be achieved through tailored activation or surface modification strategies.

Table 7
Comparison of CO_2 adsorption performance of KOH-activated biochars and activated carbons under similar conditions (~25–30 °C, ~1 bar).

Biochar	Activation method	S_{BET} (m^2/g)	V_T ($cm^3\ g^{-1}$)	CO_2 uptake (mmol/g, ~25–30 °C, 1 bar)	Surface functional groups	Source
Pine	KOH	1416	0.59	3.5	O-H, C═O, C═C, C-O	This work
Birch	KOH	1398	0.58	3.4	O-H, C═O, C═C, C-O	This work
Palm shell	KOH	1890	0.53	4.4	No report	[50]
Rice husk	KOH	2695	1.14	3.7	No report	[51]
Pine cone	KOH	1715	0.68	3.6	C-C, C—O, Si-H	[52]

3.3. CO_2 adsorption kinetics study on commercial activated carbon and KOH-activated biochars

The CO_2 adsorption kinetics of pine- and birch-derived biochars (carbonized at 600, 700 and 800 °C with a 3:1 KOH to biomass ratio) and a commercial activated carbon (AC) were evaluated at 30 °C using three models: Lagergren's pseudo–first-order, pseudo–second-order, and the Avrami–Erofeev equation.

Pseudo-first-order:

$$-\ln(1-\alpha) = k_1 t \tag{7}$$

Pseudo-second-order:

$$\frac{t}{\alpha} = \frac{1}{k_2} + t \tag{8}$$

Avrami-Erofeev:

$$\ln[-\ln(1-\alpha)] = n\ln t + \ln k_{AE} \tag{9}$$

where $-\alpha = \frac{q_t}{q_e}$ is the fractional conversion (adsorbent fraction) at time t, and k_1 is the pseudo-first-order rate constant (min^{-1}); k_2 is the pseudo-second-order adsorption rate constant ($g\ min^{-1}\ mg^{-1}$); k_{AE} is the kinetic constant (min^{-1}), and n is the Avrami exponent.

Fitting curves are shown in the Supplementary Material (S4). The corresponding kinetic parameters together with the linear regression coefficients (R [2]) are also provided in the Supplementary Material (ST2).

Overall, the excellent agreement of the pseudo–first-order model with experimental conversion curves—capturing both the steep initial uptake and the asymptotic approach to equilibrium—suggests that CO_2 adsorption on these biochars is dominated by physisorption on a quasi-homogeneous set of sites, with a rate proportional to the concentration of unoccupied sites. The Avrami equation, by contrast, highlights the possible contribution of simultaneous mechanisms (e.g., intraparticle diffusion plus surface adsorption), but its added complexity offers limited practical advantage over the simpler Lager formulation for design and scale-up of CO_2 capture processes.

To further investigate the adsorption mechanism, we applied the Weber–Morris intraparticle diffusion model to the CO_2 uptake data. The analysis focused on the 0.5–6 min window, capturing the active adsorption phase prior to equilibrium. The $q(t)$ vs $\sqrt{t}$ plots showed a clear two-stage behavior, and a slope-drop detection method was used to identify the transition point between the kinetic regions. The results indicate that adsorption proceeds via multiple rate-controlling steps: a rapid initial phase dominated by surface adsorption and external mass transfer, followed by a slower intraparticle diffusion–limited phase. Non-zero intercepts in the first segment further support the presence of film diffusion resistance. Detailed results and plots are provided in the Supplementary Information (S5 and ST3).

3.4. Cyclic adsorption–desorption performance

The cyclic adsorption–desorption tests for the samples were performed, including up to 10 consecutive adsorption cycles. The results showed no decline in adsorption capacity, with values remaining highly consistent across cycles. In some cases, a slight increase was observed, which may be attributed to enhanced accessibility or gradual pore activation. This confirms the stability and reusability of the materials under repeated operation. Supporting figures have been included in the Supplementary Information (S6).

4. Conclusions

In this study, the influence of carbonization temperature (600, 700, 800 °C) and KOH activation (3,1 KOH:carbon) on the structural, chemical, and CO_2 adsorption properties of pine- and birch-derived biochars is systematically evaluated. Equilibrium CO_2 isotherms at 30 °C were rigorously fitted to both the Langmuir model: pine carbon's Langmuir capacity increased from 2.1 mmol/g (600 °C) to 3.5 mmol/g (800 °C), while birch rose from 1.9 to 3.4 mmol/g.

Nitrogen physisorption (BET) corroborated these trends: specific surface as KOH activation at 800 °C transforms low-surface-area pine (313 $m^2\ g^{-1}$, 0.148 $cm^3\ g^{-1}$) and birch (351 $m^2\ g^{-1}$, 0.159 $cm^3\ g^{-1}$) biochars into micropore-rich adsorbents with surface area (S_{BET}) for pine (1416 $m^2\ g^{-1}$) and $V_T = 0.59\ cm^3\ g^{-1}$, and birch (1398 $m^2\ g^{-1}$) with $V_T = 0.58$ outperforming commercial AC. The contraction of average pore size (~0.94 → 0.83 nm) underscores the development of high-capacity microporosity ideal for CO_2 capture. FTIR spectra further demonstrated that higher activation temperatures introduced a greater density of oxygen-containing functional groups (–OH, C═O, C–O–C), which enhance CO_2 binding via dipole–quadrupole interactions and contribute to the observed increase in both capacity and affinity.

As these statements are based on semi-qualitative spectroscopic analysis only, confirmation with XPS would be meaningful.

The CO_2 adsorption kinetics of pine- and birch-derived biochars are best described by the pseudo–first-order model ($R^2 > 0.89$), indicating physisorption on homogeneous sites. The pseudo–second–order model poorly fits both early- and late-stage kinetics, while the Avrami model suggests mixed rate control but with limited practical advantage. The Weber–Morris diffusion data strongly support that the process is governed by a combination of external mass transfer and intraparticle diffusion, with the latter becoming significant in the second phase of the uptake.

Isosteric heats of adsorption (16–29 kJ mol^{-1}) confirmed the physisorptive nature of CO_2 binding. Cyclic CO_2 adsorption–desorption tests with up to nine consecutive cycles showed no measurable decline in capacity, confirming the stable performance of the biochars under repeated operation.

For practical flue-gas applications, CO_2/N_2 selectivity is a critical figure of merit because N_2 typically constitutes >70 vol% of industrial flue gases. Even though CO_2 is more strongly adsorbed on carbon surfaces (higher polarizability), competitive adsorption by N_2 and the presence of impurities such as (H_2O, SO_2, NO_x) can substantially reduce the effective CO_2 uptake and selectivity under real conditions. Reported CO_2/N_2 selectivity for carbonaceous adsorbents varies widely depending on pore structure and surface chemistry: values of the order of 3–10 have been reported at ~25 °C and 1 bar for different KOH-activated carbons and related porous carbons, with much higher selectivity observed at low partial pressures for ultra-micropore-rich materials[53,54,55]. Nitrogen-containing surface functionalities such as pyridinic groups have been shown to increase CO_2 affinity and selectivity through acid–base interactions, while moisture and acidic gases (SO_2, NO_x) tend to reduce capacity and accelerate deactivation [54,55,56]. Because the present study was performed with pure CO_2/He, these competitive effects were not considered in this study. Mixed-gas ($CO_2/N_2 \pm H_2O$, SO_2, NO_x) measurements are nevertheless a key prerequisite to validate the materials for industrial flue-gas capture. Another important aspect for practical application would be the consideration of the techno-economic feasibility of the activation process. The following study reports techno-economic data for activated bamboo biochar [12]; a similar study would also be required for biochar from pine and birch.

CRediT authorship contribution statement

Selma Kuloglija: Writing – review & editing, Writing – original draft, Visualization, Validation, Software, Methodology, Investigation, Formal analysis, Data curation, Conceptualization. **Ilias-Maximilian Kropik:** Visualization, Investigation, Formal analysis. **Amal El Gohary Ahmed:** Writing – review & editing, Supervision, Formal analysis, Data curation. **Viktor Kalman:** Formal analysis, Data curation. **Alexander Windbacher:** Investigation. **Christian Jordan:** Supervision, Formal analysis. **Aneta Konior:** Investigation. **Nastaran Abbaspour:**

Resources. **Noah Steinacher:** Formal analysis. **Franz Winter:** Writing – review & editing, Resources. **Daniela Tomasetig:** Formal analysis. **Elissavet Lamprinidou:** Investigation, Formal analysis. **Michael Harasek:** Writing – review & editing, Supervision.

Declaration of competing interest

The authors declare that they have no known competing financial interests or personal relationships that could have appeared to influence the work reported in this paper.

Acknowledgments

This research was funded by the Austrian Science Fund (FWF) I 5404-N. For open access purposes, the author has applied a CC BY public copyright license to any author accepted manuscript version arising from this submission. The authors acknowledge TU Wien Bibliothek for financial support through its Open Access Funding Programme. During the preparation of this work, Selma Kuloglija utilized Grammarly to enhance readability and language in the introduction.

Appendix A. Supplementary data

Supplementary data to this article can be found online at https://doi.org/10.1016/j.seppur.2025.136079.

Data availability

Data will be made available on request.

References

[1] A.N. Shafawi, A.R. Mohamed, P. Lahijani, M. Mohammadi, Recent advances in developing engineered biochar for CO2 capture: An insight into the biochar modification approaches, Elsevier Ltd. 01 (2021), https://doi.org/10.1016/j.jece.2021.106869.
[2] J. Serafin, B. Dziejarski, J. Sreńscek-Nazzal, An innovative and environmentally friendly bioorganic synthesis of activated carbon based on olive stones and its potential application for CO2 capture, Sustain. Mater. Technol. 38 (2023), https://doi.org/10.1016/j.susmat.2023.e00717.
[3] J.M. Monteagudo, A. Durán, M. Alonso, A.I. Stoica, Investigation of effectiveness of KOH-activated olive pomace biochar for efficient direct air capture of CO2, Sep. Purif. Technol. 352 (2025), https://doi.org/10.1016/j.seppur.2024.127997.
[4] N.A. Rashidi, Y.H. Chai, I.S. Ismail, M.F.H. Othman, S. Yusup, Biomass as Activated Carbon Precursor and Potential in Supercapacitor Applications, Springer Science and Business Media Deutschland GmbH, 2022, https://doi.org/10.1007/s13399-022-02351-1.
[5] "The European Green Deal" 2025, doi: https://doi.org/10.2775/367077.
[6] "Creating new economic opportunities in former mining towns" 2025, doi: https://doi.org/10.2775/655272.
[7] "The production and use of energy account for more than" 2025, doi: https://doi.org/10.2775/97540.
[8] S. Kuloglija, et al., Sustainable activated carbon production from sunflower seeds via chemical activation, Sustainability 17 (6) (2025) 2568, https://doi.org/10.3390/su17062568.
[9] J. Serafin, U. Narkiewicz, A.W. Morawski, R.J. Wróbel, B. Michalkiewicz, Highly microporous activated carbons from biomass for CO2 capture and effective micropores at different conditions, J CO_2 Util 18 (2017) 73–79, https://doi.org/10.1016/j.jcou.2017.01.006.
[10] L. Cao, et al., Straw and wood based biochar for CO2 capture: adsorption performance and governing mechanisms, Sep. Purif. Technol. 287 (2022), https://doi.org/10.1016/j.seppur.2022.120592.
[11] S. Ding, Y. Liu, Adsorption of CO2 from flue gas by novel seaweed-based KOH-activated porous biochars, Fuel 260 (2020), https://doi.org/10.1016/j.fuel.2019.116382.
[12] Y. Ji, C. Zhang, X.J. Zhang, P.F. Xie, C. Wu, L. Jiang, A high adsorption capacity bamboo biochar for CO2 capture for low temperature heat utilization, Sep. Purif. Technol. 293 (2022), https://doi.org/10.1016/j.seppur.2022.121131.
[13] N. Kaya, Z. Yıldız Uzun, Investigation of effectiveness of pine cone biochar activated with KOH for methyl orange adsorption and CO 2 capture, 2025, https://doi.org/10.1007/s13399-020-01063-8/Published.
[14] J. Sreńscek-Nazzal, A. Kamińska, J. Serafin, B. Michalkiewicz, Chemical activation of banana peel waste-derived biochar using KOH and urea for CO2 capture, Materials 17 (4) (Feb. 2024), https://doi.org/10.3390/ma17040872.
[15] X. Tan, et al., Application of biochar for the removal of pollutants from aqueous solutions, Elsevier Ltd. 01 (2015), https://doi.org/10.1016/j.chemosphere.2014.12.058.
[16] Y. Cao, X. Wang, Y. Li, Y. Tan, J. Xing, R. Fan, A comprehensive study on low-carbon impact of distributed generations on regional power grids: A case of Jiangxi provincial power grid in China, Elsevier Ltd. 01 (2016), https://doi.org/10.1016/j.rser.2015.09.008.
[17] A. Kumar, H.M. Jena, Preparation and characterization of high surface area activated carbon from fox nut (*Euryale ferox*) shell by chemical activation with H3PO4, Results Phys 6 (2016) 651–658, https://doi.org/10.1016/j.rinp.2016.09.012.
[18] A. Andrade, F.H. Dominski, D.R. Coimbra, Scientific production on indoor air quality of environments used for physical exercise and sports practice: Bibliometric analysis, Academic Press 01 (2017), https://doi.org/10.1016/j.jenvman.2017.03.001.
[19] J.A. Menndez-Diaz, I. Martin-Gulln, Activated carbon surfaces in environmental remediation types of carbon adsorbents and their production, 2025.
[20] M. Tišma, et al., Trametes versicolor in lignocellulose-based bioeconomy: State of the art, challenges and opportunities, Elsevier Ltd. 01 (2021), https://doi.org/10.1016/j.biortech.2021.124997.
[21] A. Erdem, M. Dogru, Process intensification: activated carbon production from biochar produced by gasification highly porous carbon substances with low production costs, Johnson Matthey Technol. Rev. 65 (3) (2021) 352–365, https://doi.org/10.1595/205651320x15899664199207.
[22] H. Li, X. Dong, E.B. da Silva, L.M. de Oliveira, Y. Chen, L.Q. Ma, Mechanisms of Metal Sorption by Biochars: Biochar Characteristics and Modifications, Elsevier Ltd., 2017, https://doi.org/10.1016/j.chemosphere.2017.03.072.
[23] M. Gale, T. Nguyen, M. Moreno, K.L. Gilliard-Abdulaziz, Physiochemical properties of biochar and activated carbon from biomass residue: influence of process conditions to adsorbent properties, ACS Omega 6 (15) (2021) 10224–10233, https://doi.org/10.1021/acsomega.1c00530.
[24] O. Oginni, K. Singh, G. Oporto, B. Dawson-Andoh, L. McDonald, E. Sabolsky, Influence of one-step and two-step KOH activation on activated carbon characteristics, Bioresour. Technol. Rep. 7 (2019), https://doi.org/10.1016/j.biteb.2019.100266.
[25] D. Angin, E. Altintig, T.E. Köse, Influence of process parameters on the surface and chemical properties of activated carbon obtained from biochar by chemical activation, Bioresour. Technol. 148 (2013) 542–549, https://doi.org/10.1016/j.biortech.2013.08.164.
[26] N.T. Abdel-Ghani, G.A. El-Chaghaby, M.H. Elgammal, E.S.A. Rawash, Optimizing the preparation conditions of activated carbons from olive cake using KOH activation, Xinxing Tan Cailiao/New Carbon Materials 31 (5) (2016) 492–500, https://doi.org/10.1016/S1872-5805(16)60027-6.
[27] R.B. Rios, F.W.M. Silva, A.E.B. Torres, D.C.S. Azevedo, C.L. Cavalcante, Adsorption of methane in activated carbons obtained from coconut shells using H3PO4 chemical activation, Adsorption 15 (3) (2009) 271–277, https://doi.org/10.1007/s10450-009-9174-9.
[28] Ö. Şahin, C. Saka, A.A. Ceyhan, O. Baytar, Preparation of high surface area activated carbon from *Elaeagnus angustifolia* seeds by chemical activation with ZnCl2 in one-step treatment and its iodine adsorption, Separation Sci. Technol. (Philadelphia) 50 (6) (2015) 886–891, https://doi.org/10.1080/01496395.2014.966204.
[29] F. Yuliusman, S.P. Farouq, M. Fatkhurrahman Sipangkar, S.A. Putri, Preparation and characterization of activated carbon from corn stalks by chemical activation with KOH and NaOH, in: AIP Conference Proceedings, American Institute of Physics Inc., Sep. 2020, https://doi.org/10.1063/5.0014403.
[30] T. Yumak, Surface characteristics and electrochemical properties of activated carbon obtained from different parts of *Pinus pinaster*, Colloids Surf. A Physicochem. Eng. Asp. 625 (2021), https://doi.org/10.1016/j.colsurfa.2021.126982.
[31] L. Deng, et al., Straw-based biochar prepared from multi-step KOH activation and its structure-effect relationship of CO2 capture under atmospheric/pressurized conditions via experimental analysis and MD/DFT calculations, Chem. Eng. J. 495 (2024), https://doi.org/10.1016/j.cej.2024.153403.
[32] J. Serafin, et al., Direct conversion of biomass to nanoporous activated biocarbons for high CO2 adsorption and supercapacitor applications, Appl. Surf. Sci. 497 (2019), https://doi.org/10.1016/j.apsusc.2019.143722.
[33] C. Zhang, W. Song, Q. Ma, L. Xie, X. Zhang, H. Guo, Enhancement of CO2 capture on biomass-based carbon from black locust by KOH activation and Ammonia modification, Energy Fuel 30 (5) (2016) 4181–4190, https://doi.org/10.1021/acs.energyfuels.5b02764.
[34] H.M. Coromina, D.A. Walsh, R. Mokaya, Biomass-derived activated carbon with simultaneously enhanced CO2 uptake for both pre and post combustion capture applications, J Mater Chem A Mater 4 (1) (2015) 280–289, https://doi.org/10.1039/c5ta09202g.
[35] M. Sevilla, A.B. Fuertes, Sustainable porous carbons with a superior performance for CO2 capture, Energy Environ. Sci. 4 (5) (2011) 1765–1771, https://doi.org/10.1039/c0ee00784f.
[36] S.M. Hong, E. Jang, A.D. Dysart, V.G. Pol, K.B. Lee, CO2 capture in the sustainable wheat-derived activated microporous carbon compartments, Sci. Rep. 6 (2016), https://doi.org/10.1038/srep34590.
[37] N. Abbaspour, A. Szlęk, F. Winter, A. Korus, Kinetics of model tar decomposition over activated biochar from a heavy metal-contaminated area, Renew. Energy 253 (2025), https://doi.org/10.1016/j.renene.2025.123661.

[38] N. Abbaspour, et al., Activated biochars from heavy metal-contaminated biomass for CO2 capture: adsorption performance and dominant mechanisms, J CO_2 Util 101 (2025) 103217, https://doi.org/10.1016/j.jcou.2025.103217.
[39] K. Li, et al., Insights into CO2 adsorption on KOH-activated biochars derived from the mixed sewage sludge and pine sawdust, Sci. Total Environ. 826 (2022), https://doi.org/10.1016/j.scitotenv.2022.154133.
[40] O.A. Hussain, A.S. Hathout, Y.E. Abdel-Mobdy, M.M. Rashed, E.A. Abdel Rahim, A. S.M. Fouzy, Preparation and characterization of activated carbon from agricultural wastes and their ability to remove chlorpyrifos from water, Toxicol. Rep. 10 (2023) 146–154, https://doi.org/10.1016/j.toxrep.2023.01.011.
[41] C. Spreadbury, R. Rodriguez, D. Mazyck, Comparison between FTIR and Boehm Titration for Activated Carbon Functional Group Quantification, 2017.
[42] K. Li, et al., Insights into CO2 adsorption on KOH-activated biochars derived from the mixed sewage sludge and pine sawdust, Sci. Total Environ. 826 (2022), https://doi.org/10.1016/j.scitotenv.2022.154133.
[43] Z. Tang, et al., Ultra-microporous biochar-based carbon adsorbents by a facile chemical activation strategy for high-performance CO2 adsorption, Fuel Process. Technol. 241 (2023), https://doi.org/10.1016/j.fuproc.2022.107613.
[44] J. Skubiszewska-Zięba, B. Charmas, M. Kołtowski, P. Oleszczuk, Active carbons from waste biochars: structural and thermal properties, J. Therm. Anal. Calorim. 130 (1) (2017) 15–24, https://doi.org/10.1007/s10973-017-6143-5.
[45] J.H.F. de Jesus, T.T. Da, G. Da, A.S. Mangrich, L.P.C. Romao, Adsorption of aromatic compounds by biochar: influence of the type of tropical biomass precursor, Cellulose 26 (7) (2019) 4291–4299, https://doi.org/10.1007/s10570-019-02394-0.
[46] A. Villardon, A. Alcazar-Ruiz, F. Dorado, L. Sanchez-Silva, Enhancing carbon dioxide uptake in biochar derived from husk biomasses: optimizing biomass particle size and steam activation conditions, J. Environ. Chem. Eng. 12 (5) (2024), https://doi.org/10.1016/j.jece.2024.113352.
[47] F. Sher, S.Z. Iqbal, S. Albazzaz, U. Ali, D.A. Mortari, T. Rashid, Development of biomass derived highly porous fast adsorbents for post-combustion CO2 capture, Fuel 282 (2020), https://doi.org/10.1016/j.fuel.2020.118506.
[48] Y. Luo, J. Street, P. Steele, E. Entsminger, V. Guda, Activated carbon derived from pyrolyzed pinewood char using elevated temperature, KOH, H 3 PO 4, and H 2 O 2, 2025.
[49] K. Li, S. Tian, J. Jiang, J. Wang, X. Chen, F. Yan, Pine cone shell-based activated carbon used for CO2 adsorption, J Mater Chem A Mater 4 (14) (2016) 5223–5234, https://doi.org/10.1039/c5ta09908k.
[50] A.S. Ello, L.K.C. De Souza, A. Trokourey, M. Jaroniec, Development of microporous carbons for CO2 capture by KOH activation of African palm shells, J CO_2 Util 2 (2013) 35–38, https://doi.org/10.1016/j.jcou.2013.07.003.
[51] D. Li, T. Ma, R. Zhang, Y. Tian, Y. Qiao, Preparation of porous carbons with high low-pressure CO2uptake by KOH activation of rice husk char, Fuel 139 (2015) 68–70, https://doi.org/10.1016/j.fuel.2014.08.027.
[52] N. Kaya, Z. Yıldız Uzun, Investigation of effectiveness of pine cone biochar activated with KOH for methyl orange adsorption and CO 2 capture, 2020, https://doi.org/10.1007/s13399-020-01063-8/Published.
[53] R. Nandi, M.K. Jha, S.K. Guchhait, D. Sutradhar, S. Yadav, Impact of KOH activation on Rice husk derived porous activated carbon for carbon capture at flue gas alike temperatures with high CO2/N2 selectivity, ACS Omega 8 (5) (Feb. 2023) 4802–4812, https://doi.org/10.1021/acsomega.2c06955.
[54] V. Selmert, A. Kretzschmar, H. Weinrich, H. Tempel, H. Kungl, R.A. Eichel, CO2/N2 separation on highly selective carbon nanofibers investigated by dynamic gas adsorption, ChemSusChem 15 (14) (Jul. 2022), https://doi.org/10.1002/cssc.202200761.
[55] S.K. Bhatia, Density functional theory analysis of the influence of pore wall heterogeneity on adsorption in carbons, Langmuir 18 (18) (Sep. 2002) 6845–6856, https://doi.org/10.1021/la0201927.
[56] M. Karimi, M. Shirzad, J.A.C. Silva, A.E. Rodrigues, Carbon dioxide separation and capture by adsorption: a review, Springer Science and Business Media Deutschland GmbH 01 (2023), https://doi.org/10.1007/s10311-023-01589-z.